An Empirical Comparison of Modulation Schemes in Turbulent Underwater Optical Wireless Communications

An Empirical Comparison of Modulation Schemes in Turbulent Underwater Optical Wireless Communications

Callum T. Geldard, Egecan Guler, Alexander Hamilton and Wasiu O. Popoola, *Senior Member, IEEE*

***Abstract*—This paper presents an empirical comparison of different modulation schemes in still and turbulent water conditions. Using an underwater channel emulator, it is shown that pulse position modulation (PPM) and subcarrier intensity modulation (SIM) have an inherent resilience to turbulence induced fading with SIM achieving higher data rates under all conditions. Finally, the signal processing technique termed pairwise coding (PWC) is applied to SIM in underwater optical wireless communications for the first time. The performance of PWC is compared with the, state-of-the-art, bit and power loading optimisation algorithm. Using PWC, a maximum data rate of 5.2 Gbps is achieved in still water conditions.**

I. Introduction

Underwater optical wireless communications (UOWC) is an application in the field of optical wireless communications (OWC). Due to the nature of light, UOWC has some inherent advantages over the dominant underwater acoustic communications (UAC). These include lower latency and higher data rates, albeit over shorter link distances [1]. These advantages, coupled with the lower transmission power associated with the semiconductor devices used in OWC, can enable remote high speed wireless communication over tens of metres. As such, UOWC could form a complementary hybrid network along with the UAC and radio frequency modes of transmission. The removal of cables, typically used for high speed communications, could save time and money for retrieving data from sensor nodes in coastal water or the open sea, ships in a harbour, and for communication with remotely operated vehicles.

In order for a reliable UOWC system to be developed, the channel must be understood. Prior works have examined channel characterisation through empirical studies. These investigations can be categorised as those that study the still water channel, as in references [2]–[4], and those that focus on the turbulent channel, as in references [5]–[9]. This knowledge of the channel characteristics can be used in system design to overcome the performance limitations imposed by the channel. When developing an UOWC system for a particular application, the power and data rate requirements must be considered along with which modulation scheme is to be used. These considerations cannot be made without an understanding of the performance of different modulation schemes in different channel conditions.

Callum T. Geldard, Egecan Guler, and Wasiu O. Popoola are with the School of Engineering, The University of Edinburgh, Edinburgh EH9 3JL, U.K. Alexander Hamilton is with the UK Defence Science and Technology Laboratory (DSTL). (e-mails: callum.geldard@sms.ed.ac.uk; s1553558@ed.ac.uk; w.popoola@ed.ac.uk).

The paper is organised as follows: section II outlines the contributions to knowledge made by this work relative to existing literature; section III provides a brief insight into the UOWC channel; section IV gives a description of the modulation schemes used in this paper; section V describes the experimental setup including the underwater channel emulator (UCE); section VI contains a brief characterisation of the channel used in this work; section VII details the performance of data transmitted through the UCE using each modulation scheme; in section VIII, signal processing techniques are applied to overcome the bandwidth limitations of the system; and section IX draws conclusions.

II. Contributions and Relation to State-of-the-Art

The majority of experimental works in literature are focused on characterising turbulence in the channel or data transmission in still waters. To the best of the authors knowledge there exists no work that details comparative data transmission through turbulent underwater channel. Works in literature have, however, examined the impact of bubble concentration on the error performance of UOWC [10], [11]. This paper presents an empirical study of data transmission in the turbulent underwater channel and considers a wide range of modulation techniques. This is complementary to existing works in literature.

The modulation schemes under test are: pulse amplitude modulation (PAM); pulse position modulation (PPM); and subcarrier intensity modulation (SIM), with both phase shift keying (PSK) and quadrature amplitude modulation (QAM). As part of this contribution, we present empirically measured bit error rate (BER) performance in underwater turbulent conditions. This is the first time in literature that comparative BER curves for different modulation schemes have been presented in underwater turbulence. The framework used to take these BER measurements is briefly described in this paper also. Additionally, signal processing techniques are applied to the SIM transmission to improve performance. These are pairwise coding (PWC) and bit and power loading. The two techniques are applied in both still and turbulent water conditions.

The state-of-the-art in UOWC in terms of data rate is 30 Gbps. This was achieved in still, fresh water using

PAM [12]. This data rate was achieved over 12.5 m link, and in the same study, 15 Gbps was achieved over a 2.5 m turbid link. Additionally, 12.8 Gbps [13] and 20 Gbps [14] have been achieved using orthogonal frequency division multiplexing (OFDM) and discrete multitone transmission respectively, these are both variations of the SIM scheme covered in this study. The OFDM technique was further developed to incorporate wavelength and polarisation diversity to achieve 26.9 Gbps in reference [15].

The data rates and link distance achieved in this study are lower than those used in the state of the art works. However, the focus of our work is to examine the performance of data transmission through the turbulent UOWC channel. Therefore, the purpose of this study is to evaluate performance in turbulent underwater channel conditions.

III. The Underwater Optical Wireless Communication Channel

UOWC systems have to contend with the inherent optical properties (IOP) of water. These IOP are defined in terms of absorption and scattering of still water [16]. Another important effect is turbulence, that can be understood as a case of random scattering. It is caused by fluctuations in the temperature and salinity, yielding changes in refractive index along the channel [17]. As the photon beam deviates from its initial path, the number arriving at the receiver decreases. This phenomena is known as turbulence induced fading.

After propagating through a channel with turbulence induced fading, the received signal, $y(t)$, is given by:

$$y(t) = \alpha \mathcal{R} P_{\mathrm{t}}(t) h(t) + n(t), \tag{1}$$

where, $P_{\mathrm{t}}(t)$ is the transmitted signal power at time t, $\mathcal{R}$ is the responsivity of the photodetector, $h(t)$ represents the channel impulse response, and $n(t)$ is additive noise. Here, the effect of turbulence is modelled by a random fading variable, α. A commonly used model to represent the probability density function (PDF) of the underwater turbulence fading parameter, α, is the Log-Normal distribution. It is given as [18]:

$$P_{\alpha}(\alpha) = \frac{1}{\alpha \sigma_{\alpha} \sqrt{2\pi}} \exp\left(-\frac{(\ln \alpha - \mu)^2}{2\sigma_{\alpha}^2} \right), \tag{2}$$

where μ is the mean of $\ln \alpha$, and σ_{α}^2 is the variance of the random multiplicative fading variable α.

The impact of turbulence induced fading on a received signal can be quantified in terms of the scintillation index, σ_I^2, defined as [1]:

$$\sigma_I^2 = \frac{\langle I^2 \rangle - \langle I \rangle^2}{\langle I \rangle^2}, \tag{3}$$

where I is the received optical intensity and $\langle . \rangle$ denotes the ensemble average. As I is proportional to α then σ_{α}^2 is also proportional to σ_I^2.

IV. Modulation Schemes

This section will briefly introduce the modulation schemes considered in this work and comment on their merits. These are selected due to their use in literature in terrestrial and underwater OWC and are all intensity modulated with direct detection (IM/DD). Data is encoded within the characteristics of this time continuous IM transmitted optical signal.

One such characteristic is the amplitude. In PAM, data is carried in the amplitude of the signal [19]. In its simplest form, unipolar 2-PAM is the same as on-off keying (OOK). The OOK scheme has been widely reported in literature, including [20], [21]. The spectral efficiency can be increased by adding additional amplitude levels to the signal, i.e. increasing the modulation order, M. This was demonstrated in the state of the art work, which utilised PAM with $M = 4$ in [12]. However, turbulence induced fading causes the received signal amplitude to vary over time. This in turn causes the decision boundary between symbols to change continuously in the presence of turbulence. The effect of this can be alleviated by the use of adaptive thresholding (AT) at the receiver. When using AT, channel state information (CSI) is regularly updated over the course of transmission. This up-to-date CSI, is then used when decoding the received signal. This is in contrast to fixed threshold (FT) decoding, where CSI taken prior to transmission is used to decode all symbols. In a constantly changing turbulent channel, AT can be expected to outperform FT. However, the requirement of accurate CSI adds complexity to the AT system design.

One alternative to amplitude modulation is to encode the data on the position of a pulse within the symbol period, as in PPM [19]. Here, the amplitude of the transmitted pulse is constant. So, the data is shielded from the effects of fading. For this reason, PPM is suited to applications where knowledge of the channel may be limited, as in the turbulent fading channel. PPM was implemented in UOWC in reference [22]. Compared to PAM, PPM is not spectrally efficient due to the symbol structure. So, it is not suited to applications with a bandwidth limitation.

The third technique under test is SIM; here data carrying subcarriers are separately modulated with data encoded in the phase and/or the amplitude of each subcarrier [19]. When the data is encoded on the phase, as in PSK-SIM, CSI is not required at the receiver. Spectral efficiency may be further increased by encoding data on the amplitude in addition to the phase, as in QAM-SIM. However, as in PAM, there is a trade-off in terms of the requirement of accurate CSI when decoding an amplitude modulated signal. BPSK modulated SIM has been shown to be resilient to turbulence in terrestrial OWC in both simulation [23] and experimental studies [24]. It has also been applied in still water UOWC in [25].

Most practical systems will have frequency selectivity introduced by the inherent properties of the communication front-end devices, components, and/or the channel. In this case, SIM with multiple subcarriers will experience an imbalance in signal-to-noise-ratio (SNR) across different subcarriers. This imbalance can be mitigated using signal processing techniques. The techniques used in this paper are PWC and bit and power loading. PWC is a signal space diversity technique that can alleviate this SNR imbalance and help improve the overall system performance [26]. Alternatively, bit and power loading uses the CSI to assign a higher M to the subcarriers with high SNR and a lower M to those with low SNR. This process is

used to maximise the data rate in a given channel [27].

V. Experimental Setup

A block diagram illustrating the experimental set up used in this study is shown in Fig. 1. Using Matlab software, random data is generated and modulated using the previously mentioned modulation schemes. These modulated data streams are then sent to the Keysight m8195a arbitrary waveform generator (AWG). The signal is then transmitted from the AWG via a Thorlabs PL450b laser diode (LD) with a peak-to-peak voltage of 0.5 V. A DC current of 30 mA is added to the signal using a diplexer (bias-T), in order to keep the LD operating above its threshold current. This optical signal is then collimated and transmitted through the UCE. At the receiver, the optical signal is recovered by a New Focus 1601 photo-diode and the resulting electrical signal is sampled by an Agilent DSA90804A oscilloscope. This sampled signal is then recovered and decoded off-line using Matlab.

The UCE consists of a large aquarium style water tank with dimensions $1.5 \times 0.5 \times 0.5$ m^3 and is filled with 225 L of tap water. In this work, a temperature gradient is applied by controlling the heat source to generate turbulence within the link, as in our earlier work [5]. The UCE is set up with a heater positioned in the centre of the tank, perpendicular to the propagation path of the collimated laser beam.

For this experimental work, three different conditions of weak turbulence are used: still water with a temperature gradient, $\Delta T \approx 0$ K and $\sigma_I^2 \approx 0$; turbulence condition 1 with $\Delta T \approx 6$ K and $\sigma_I^2 \approx 0.1$; and turbulence condition 2 with $\Delta T \approx 10$ K and $\sigma_I^2 \approx 0.3$. The channel in condition 1 is very controllable so could be held at $\sigma_I^2 = 0.1 \pm 0.05$, whilst, towards the top end of this set up, condition 2 is much more difficult to hold to a precise value resulting in the large variation between $\sigma_I^2 = 0.3 \pm 0.1$ for this condition. As a result of this variation in condition 2 turbulence strength, the analysis of modulation schemes will focus on still water and turbulence condition 1. The results obtained through turbulence condition 2 will be used for comparing the maximum supported data rate only. The turbulence considered in this work is in the weak regime, as the scintillation index is less than unity.

VI. Channel Evaluation

Using the experimental set up described in Section V, the channel is characterised in order to aid the understanding of the data transmission through it. The average received SNR is approximately 27 dB in still water. Fig. 2 shows the normalised frequency response of the system. The -3 dB bandwidth extends beyond 1 GHz but there is a drop to just above -3 dB between approximately 750 and 950 MHz before

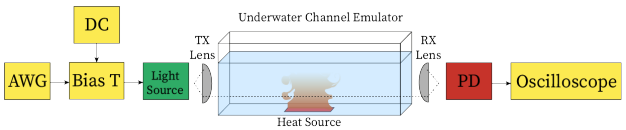

Fig. 1: The system block diagram used in this study including the underwater channel emulator.

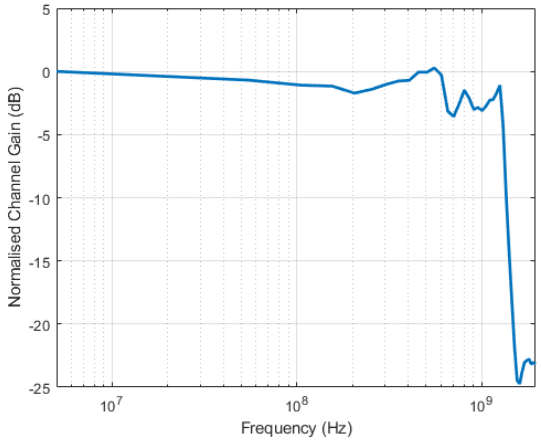

Fig. 2: The normalised frequency response of the system in still water. The measured system bandwidth is limited by the photodetector used.

the gain increases towards 1.2 GHz. Beyond 1.2 GHz there is a steep roll-off with the channel gain dropping to a floor around -25 dB. The bandwidth limitation displayed in the frequency response is predominantly caused by the photodiode used in the system.

The turbulence generated in the UCE is measured and characterised prior to data transmission, using the process described in [5]. The received intensity distributions are fitted with Gaussian and Log-Normal functions. The goodness of these fits is quantified using the R^2 metric, where a value of $R^2 = 1$ denotes a function that perfectly describes the data set. Fig. 3 shows the received signal distributions for still water and turbulence conditions 1 ($\sigma_I^2 = 0.15$) and 2 ($\sigma_I^2 = 0.35$). The still water distribution is centred around a mean normalised received peak-to-peak voltage, V_{pp}, of 1 and has a Gaussian shape with $R^2 = 0.96$. As the σ_I^2 is low, the distribution is tight around the mean. The distribution from turbulence condition 1 on the other hand has a mean $V_{\text{pp}} \approx 0.8$ which corresponds to a drop in the mean received SNR. The σ_I^2 is also greater, meaning there is more variation in the received signal. With turbulence, a Gaussian fit no longer best describes the distribution. Here, the Log-Normal function provides a better fit. This is evidenced by the R^2 values for the fitted Gaussian and Log-Normal curves in Fig. 3b, they are 0.96 and 0.98 respectively. The difference in distribution shapes is further highlighted in turbulence condition 2. Here, the R^2 of the Gaussian fit is 0.89 compared to 0.97 for Log-Normal. This suggests that as the strength of turbulence increases, the distributions become less Gaussian in shape.

VII. Data Transmission Through a Turbulent UOWC

The turbulence generated in the UOWC channel emulator results in slow fading. This means it is non-varying over the sampling interval of the data logger (oscilloscope, DSA90804A). Therefore, in order to gain an understanding of the BER performance of a turbulent channel, data is transmitted as packets of 80×10^3 samples for 1000 iterations.

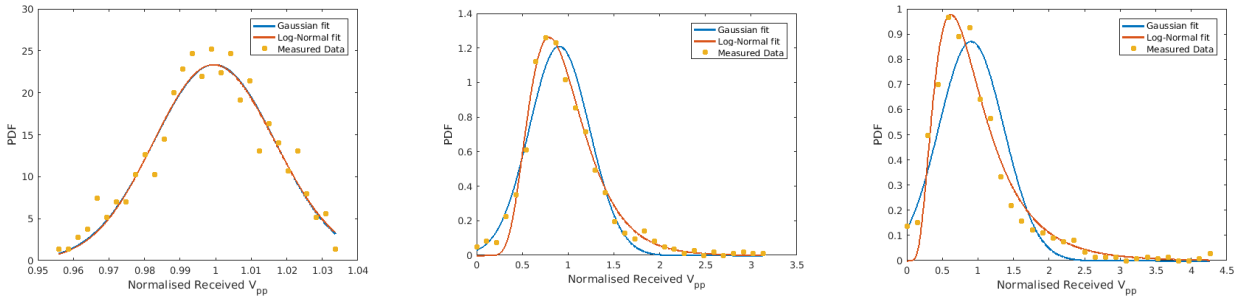

(a) $\sigma_I^2 = 2.87 \times 10^{-4}$ (b) $\sigma_I^2 = 0.15$ (c) $\sigma_I^2 = 0.35$

Fig. 3: Received intensity distributions measured using the channel emulator fitted with Gaussian and Log-Normal curves in still and turbulent waters.

This ensures that for each modulation scheme, the BER of the random channel will converge to a repeatable value for a given σ_I^2, M, and symbol rate, R_s. Throughout this experiment, the sample rate, F_s, is fixed to 40 Gsamp/s. This is because the the m8195a AWG only allows for F_s of $\{64; 32; 16\}$ Gsamp/s. To account for this, the signal is generated based on $F_s = 40$ Gsamp/s, then up-sampled to 64 Gsamp/s for transmission. The oscilloscope samples at a rate of 40 Gsamp/s to recover the original signal. Therefore, in order to control R_s, the oversampling factor is changed while F_s is kept constant.

A. Image Transmission

To illustrate the effect of turbulence on the transmission of data, an image is converted into a bit stream and transmitted through the UCE. The decoded images, transmitted using 2-PAM and 2-PSK-SIM, are displayed in Fig. 4 along with the original image. In the still water channel, the original image is recoverable with both modulation schemes - albeit with a small amount of distortion with 2-PSK-SIM. However, the images recovered from transmission through the turbulent channel show a stark contrast between the schemes. The image transmitted using 2-PSK-SIM has a few blemishes but the original image can still clearly be picked out. The image transmitted using 2-PAM on the other-hand, is heavily distorted. The colouring is incorrect as the red-green-blue values for each pixel experience a different channel fade. Visually, it is difficult to make out what the image is in this case. This clearly demonstrates the effect of underwater turbulence on PAM and the resilience of PSK-SIM to turbulence.

B. PAM Transmission

Fig. 5 shows the BER against R_s curves for $\{2, 4\}$-PAM in still water and in the turbulence condition 1 with $\sigma_I^2 \approx 0.1$. It is shown in Fig. 5 that in still water for 2-PAM, AT decoding has slightly better error performance than FT. However, when the data is transmitted through a turbulent channel, 2-PAM with FT approaches an error floor of 6×10^{-2}. Whereas, with adaptive decoding only a small drop in performance is experienced. The forward error correction (FEC) limit of 3×10^{-3} is reached at approximately 2.7 Gsym/s in turbulence compared to 2.9 Gsym/s in still water. This suggests that AT is required in order to successfully transmit data through a turbulent channel when using PAM. Note that at the FEC limit BER or lower, channel coding techniques can be used to make the transmission effectively error free.

In order to increase the number of bits per symbol, a higher order of PAM can be used. Using 4-PAM in still water, the symbol rate at the FEC limit is breached is around 800 Msym/s, yielding a data rate of 1.6 Gbps. Which is lower than the 2.9 Gbps achievable with 2-PAM. This suggests that the channel bandwidth and SNR limitations mean that higher orders of M-PAM cannot be supported. Furthermore, even with adaptive decoding, the channel cannot support 4-PAM in the turbulence condition 1.

C. PPM Transmission

Shown in Fig. 6 are the BER versus R_s curves for $\{2, 4, 16\}$-PPM in the still water channel as well as in turbulence condition 1 with $\sigma_I^2 \approx 0.1$. Here, the resilience to turbulence of PPM is shown clearly. There is no noticeable difference between the error performance in still and turbulent channels. There seems to be an anomaly in the 2-PPM results, whereby there is a difference in performance between the still and turbulent channels. Here, the BER performance in the turbulent channel is slightly better than the still channel above 1.4 Gsym/s. This happens when the BER is too high (above the FEC limit of 3×10^{-3}) for any reliable communication to be established. However, 2-PPM is error free below 1.4 Gsym/s in still water, whereas this is not the case in turbulence condition 1. This anomalous result at high BER can be attributed to the random nature of the channel.

In order to increase the number of bits per symbol in PPM, the number of time slots occupied by a symbol must be increased. Therefore for the same channel bandwidth, the achievable symbol rate drops as the number of bits per symbol increases. This is shown to be the case in Fig. 6, where 2, 4, and 16 PPM reach the FEC limit at 1.4 Gsym/s, 750 Msym/s, and 300 Msym/s respectively. However, these symbol rates yield respective bit rates of 1.4 Gbps, 1.5 Gbps, and 1.2 Gbps. It should be noted that 16-PPM requires much higher bandwidth than 2, or 4-PPM. But the UCE link used in this study has limited bandwidth as shown in Fig. 2. The additional distortion suffered by 16-PPM as a result of the

(a) Original image.

(b) 2-PAM in still water.

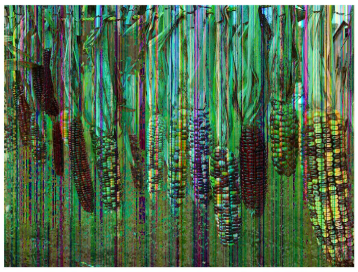

(c) 2-PAM in turbulence.

(d) 2-PSK-SIM in still water.

(e) 2-PSK-SIM in turbulence.

Fig. 4: Decoded image after propagating through the UCE using both 2-PAM and 2-PSK-SIM at 1 Gbps data rate.

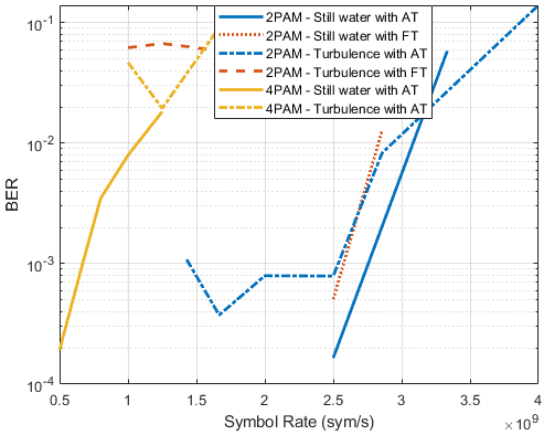

Fig. 5: BER curve for M-PAM transmission in still and turbulent ($\sigma_I^2 \approx 0.1$) water channels, using adaptive (AT) and fixed (FT) threshold decoding.

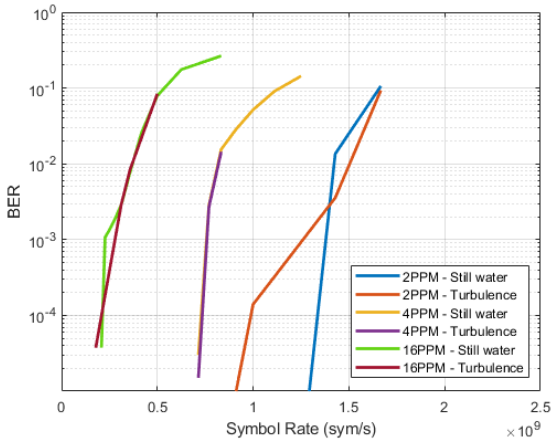

Fig. 6: BER curve for M-PPM transmission in still and turbulent ($\sigma_I^2 \approx 0.1$) water channels.

bandwidth limitation is responsible for its lower bit rate at the FEC limit.

D. SIM Transmission

SIM encoded data is transmitted through the UCE across 64 subcarriers. The curves of BER versus R_s for SIM with $\{2, 4, 8, 16, 32\}$-PSK are shown in Fig. 7. For $M = 2$, 4, and 8 there is a small drop in performance between the still and turbulent channels owing to the fall in average SNR associated with turbulence induced fading. Here, the data is encoded on the phase of the signal, so despite this drop in average SNR, up to $M = 8$ can be supported in the turbulent channel below the FEC limit. This can be contrasted to PAM, which cannot support $M > 2$ in turbulence. In the turbulent channel, the maximum supported data rate is 3.36 Gbps, achieved with $M = 8$. This can be compared to a rate of 3.4 Gbps in the still water channel. In still water, PSK-SIM can support up to $M = 32$ at FEC limit, but in the turbulence condition it can only support orders up to $M = 8$.

Higher order modulation can be accommodated by encoding data onto the amplitude as well as the phase of the transmitted signal. This is shown in Fig. 8 where SIM is modulated with $\{4, 16, 64\}$-QAM in still and turbulent waters. As with PSK-SIM, QAM modulated SIM experiences an increase in BER for a given symbol rate in the presence of turbulence compared to the still channel. In still water, a maximum data rate of 4.2 Gbps is reached with 16-QAM and there is no

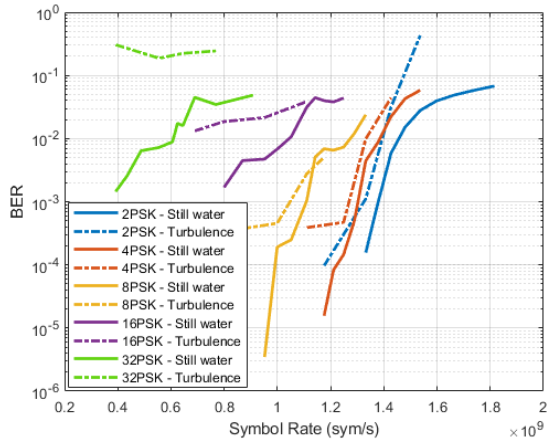

Fig. 7: BER curve for PSK-SIM transmission in still and turbulent ($\sigma_I^2 \approx 0.1$) water channels.

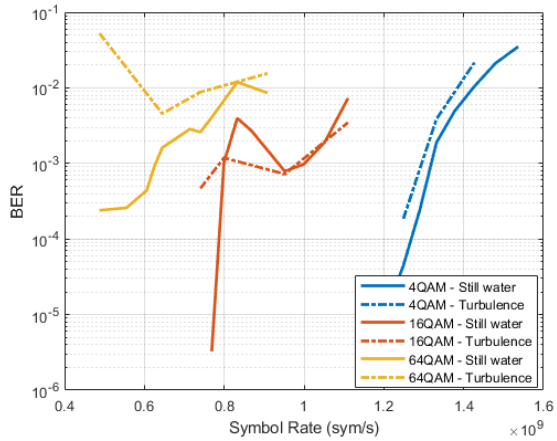

Fig. 8: BER curve for QAM-SIM transmission in still and turbulent ($\sigma_I^2 \approx 0.1$) water channels.

clear drop in rate when turbulence is applied to the channel. The greater separation between symbols in QAM (and the additional dimension upon which data is modulated) means its SNR requirement is lower than in PSK-SIM of the same order for $M > 4$. Resultantly, at the FEC BER or lower, modulation orders up to $M = 64$ can be supported in still water and $M = 16$ in the turbulent condition.

In Fig. 7 and 8, the BER curves display a stepped shape when $M > 2$. This is most noticeable for 16-QAM-SIM in Fig. 8 where, in both channel conditions, there is a dip in BER at approximately 0.8 Gsym/s followed by an increase above 0.9 Gsym/s. We believe this is a consequence of the fluctuation in the channel response at around 0.6 GHz-1 GHz, as shown in Fig. 2.

E. Comparison of PAM, PPM and SIM Schemes

The comparison of the different modulation and signal processing techniques used in this study is summarised in Fig. 9. The maximum data rate attained at the FEC limit of BER $\leq 3 \times 10^{-3}$ is obtained from the BER versus R_s

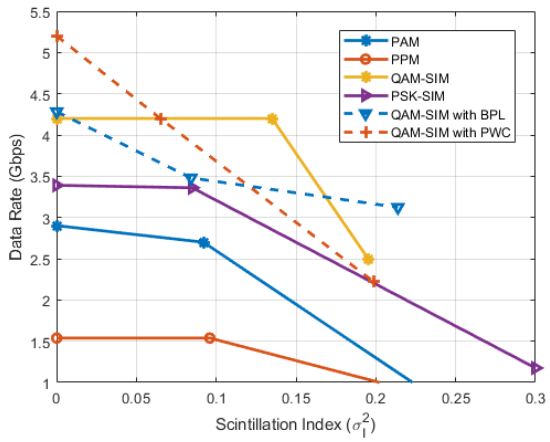

Fig. 9: A comparison of the maximum data rate achieved to $BER \leq 3 \times 10^{-3}$ using each modulation scheme in different channel conditions.

curves for each scheme. It is shown that in still water, with $\sigma_I^2 \approx 0$, the maximum data rate is 5.2 Gbps achieved using QAM-SIM with PWC. The maximum data rate achieved in turbulence condition 1, $\sigma_I^2 \approx 0.1$, is 4.2 Gbps using SIM with 16-QAM. Finally, in turbulence condition 2, the highest data rate is obtained via QAM-SIM with bit and power loading to achieve 3.1 Gbps. It can be noted that, as σ_I^2 increases, the performance of PWC degrades at a steeper rate than the other schemes under test. QAM-SIM with bit and power loading also degrades in turbulence condition 1 at a faster rate than basic-SIM as the subcarrier loading is based on an average CSI in a changing channel.

The inherent resilience of SIM and PPM to turbulence is further emphasised in Fig. 9 where the drop in maximum rate between still water and the turbulence condition 1 is shown to be small compared to PAM. There is very little or no difference between the maximum data rates attainable in still water and in turbulence condition 1 for the SIM and PPM schemes. The turbulence condition 2 is included to show the limits of this resilience. When σ_I^2 is higher, the likelihood of a deep fade is higher, thus, the BER will increase. Additionally, as σ_I^2 increases, the mean SNR decreases - as illustrated in Fig. 3 - further reducing the maximum achievable data rate. Here, bit and power loading has an advantage over the basic-SIM. With the bit loading optimisation algorithm, the number of bit loaded onto a subcarrier, M_i, is calculated based on the mean SNR estimated using pilot bits. So, the reduced SNR per subcarrier is accounted for. It is worth emphasising that bit/power loading requires an accurate knowledge of the channel conditions.

VIII. Signal Processing Techniques to Overcome Bandwidth Limitations

Additional signal processing techniques may be applied to these modulation schemes in order to further improve performance. However, due to the accurate CSI required to perform these signal processing techniques, they are presented for discussion in still water only.

A. SIM with Pairwise Coding

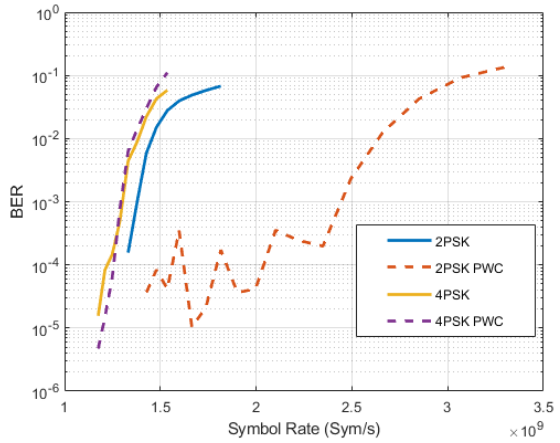

Fig. 10: BER curve for PSK-SIM-PWC transmission in the still water channel.

PWC is applied to SIM to overcome bandwidth limitations in the system. Fig. 10 shows the BER performance of PSK-SIM with and without PWC. There is a large gain from using PWC in 2-PSK-SIM with the symbol rate at FEC increasing from approximately 1.5 Gsym/s to 2.5 Gsym/s. The gain of PWC decreases as the minimum phase difference between symbols decreases. Thus, 4-PSK-SIM with PWC does not offer any significant gain for the channel under consideration.

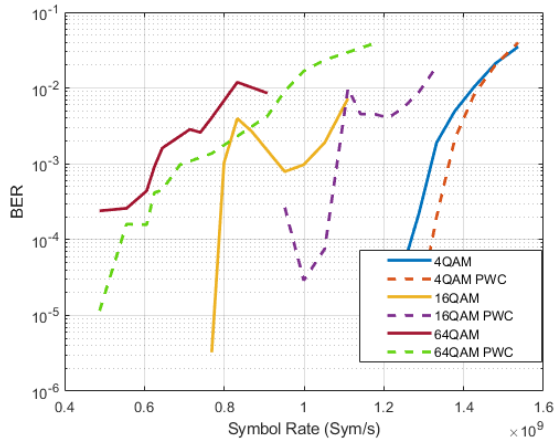

Fig. 11: BER curve for QAM-SIM-PWC transmission in the still water channel.

Shown in Fig. 11 is the empirical BER as a function of R_s for QAM-SIM with PWC. As data is encoded on both the phase and the amplitude of the transmitted signal, there is more scope for gain from phase rotation and interleaving to improve the average BER. The performance of 4-QAM-SIM should be identical to that of 4-PSK-SIM. So the very small gain observed in 4-QAM-SIM with PWC is down to experimental variations. However, the large gains from PWC in 16 and 64-QAM are in line with expectations and highlight the benefits of the technique. The symbol rates at FEC increase to approximately 1.1 Gsym/s and 870 Msym/s for 16 and 64-QAM respectively. These correspond to data rates of 4.4 Gbps and 5.2 Gbps which represent a sizeable gain over QAM-SIM without PWC in still water.

B. SIM with Bit and Power Loading

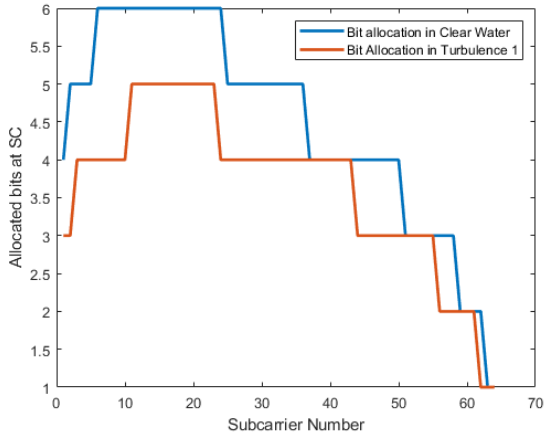

Fig. 12: The bit allocation graph for clear water and turbulence condition 1 at a symbol rate of 1 GSym/s

The graph shown in Fig. 12 displays the M_i allocated to each subcarrier with bit loading at the sampling rate of 1 Gsym/s. The maximum M_i is 6 which corresponds to 64-QAM, implying that the SNR is too low to support $M > 6$. This is in line with the basic-SIM results, where 64-QAM can only be supported below 700 Msym/s. It is shown that for the turbulent channel, fewer bits are allocated to each subcarrier. As a result of this, the total transmission speed is lower in turbulent conditions than in still waters.

IX. Conclusion

It is shown through experimental results, that modulation schemes that do not encode data on signal amplitude only - namely SIM and PPM - have an inherent resilience to turbulence induced fading. Of these, PPM is spectrally inefficient; making it unsuitable in bandwidth limited channels or for high data rate applications. Signal processing techniques are applied to the SIM scheme in order to improve its achievable data rate. The PWC offers a good improvement over basic-QAM-SIM in still waters but its performance in turbulence is worse than that of basic-SIM due to its dependence on the accurate knowledge of the channel. For the link response under consideration, bit and power loading results in marginal improvement over the uniformly-loaded QAM-SIM in still water with no turbulence. In the underwater channel with turbulence strength, $\sigma_I^2 = 0.3$, bit and power loading provides a significant gain over the basic-QAM-SIM. This is because with bit/power loading, the drop in average SNR is accounted for through the use of measured CSI in assigning modulation order to the subcarriers.

REFERENCES

[1] H. Kaushal and G. Kaddoum, "Underwater optical wireless communication," *IEEE Access*, vol. 4, pp. 1518–1547, 2016.

[2] L. Ma, M. Fu, Z. Gu, M. Sun, H. Yang, X. Ren, B. Zheng, and X. Liu, "Experiments of recreating the frequency domain properties of seawater channel for underwater optical communication," in *OCEANS 2019 - Marseille*, 2019, pp. 1–4.

[3] B. Cochenour, A. Laux, and L. Mullen, "Temporal dispersion in underwater laser communication links: Closing the loop between model and experiment," in *2016 IEEE Third Underwater Communications and Networking Conference (UComms)*, 2016, pp. 1–5.

[4] N. D. Hardy, C. E. DeVoe, A. S. Fletcher, I. D. Gaschits, F. Hakimi, H. G. Rao, T. M. Yarnall, and S. A. Hamilton, "Modeling and experimental validation of narrow beam propagation through a turbid harbor," in *OCEANS 2016 MTS/IEEE Monterey*, 2016, pp. 1–6.

[5] C. T. Geldard, J. Thompson, and W. O. Popoola, "Empirical study of the underwater turbulence effect on non-coherent light," *IEEE Photonics Technology Letters*, vol. 32, no. 20, pp. 1307–1310, 2020.

[6] M. V. Jamali, A. Mirani, A. Parsay, B. Abolhassani, P. Nabavi, A. Chizari, P. Khorramshahi, S. Abdollahramezani, and J. A. Salehi, "Statistical studies of fading in underwater wireless optical channels in the presence of air bubble, temperature, and salinity random variations," *IEEE Transactions on Communications*, vol. 66, no. 10, pp. 4706–4723, 2018.

[7] H. M. Oubei, E. Zedini, R. T. ElAfandy, A. Kammoun, M. Abdallah, T. K. Ng, M. Hamdi, M.-S. Alouini, and B. S. Ooi, "Simple statistical channel model for weak temperature-induced turbulence in underwater wireless optical communication systems," *Opt. Lett.*, vol. 42, no. 13, pp. 2455–2458, Jul 2017. [Online]. Available: http://www.osapublishing.org/ol/abstract.cfm?URI=ol-42-13-2455

[8] M. V. Jamali, P. Khorramshahi, A. Tashakori, A. Chizari, S. Shahsavari, S. AbdollahRamezani, M. Fazelian, S. Bahrani, and J. A. Salehi, "Statistical distribution of intensity fluctuations for underwater wireless optical channels in the presence of air bubbles," in *2016 Iran Workshop on Communication and Information Theory (IWCIT)*, 2016, pp. 1–6.

[9] Y. Guo, A. Trichili, O. Alkhazragi, I. Ashry, T. K. Ng, M.-S. Alouini, and B. S. Ooi, "On the reciprocity of underwater turbulent channels," *IEEE Photonics Journal*, vol. 11, no. 2, pp. 1–9, 2019.

[10] H. M. Oubei, R. T. ElAfandy, K.-H. Park, T. K. Ng, M.-S. Alouini, and B. S. Ooi, "Performance evaluation of underwater wireless optical communications links in the presence of different air bubble populations," *IEEE Photonics Journal*, vol. 9, no. 2, pp. 1–9, 2017.

[11] D. Chen, J. Wang, S. Li, and Z. Xu, "Effects of air bubbles on underwater optical wireless communication," *Chinese Optics Letters*, vol. 17, no. 10, p. 100008, 2019.

[12] W.-S. Tsai, H.-H. Lu, H.-W. Wu, C.-W. Su, and Y.-C. Huang, "A 30 Gb/s PAM4 underwater wireless laser transmission system with optical beam reducer/expander," *Scientific Reports*, vol. 9, no. 1, pp. 2045–2322, Jun 2019. [Online]. Available: https://doi.org/10.1038/s41598-019-45125-y

[13] X. Hong, C. Fei, G. Zhang, and S. He, "Probabilistically shaped 256-QAM-OFDM transmission in underwater wireless optical communication system," in *Proceedings of Optical Fiber Communication Conference 2019*. Optical Society of America, 2019. [Online]. Available: http://www.osapublishing.org/abstract.cfm?URI=OFC-2019-Th2A.40

[14] J. Du, X. Hong, Y. Wang, Z. Xu, W. Zhao, N. Lv, C. Fei, and S. He, "A comprehensive performance comparison of DFT-S DMT and QAM-DMT in UOWC system in different water environments," *IEEE Photonics Journal*, vol. 13, no. 1, pp. 1–11, 2021.

[15] Z. Wang, L. Zhang, Z. Wei, Y. Dong, G. Wei, and H. Fu, "Beyond 25 Gbps OFDM UOWC system based on green and blue laser diodes with wavelength and polarization multiplexing," in *2021 9th International Conference on Communications and Broadband Networking*, 2021, pp. 329–332.

[16] C. D. Mobley. [Online]. Available: http://www.oceanopticsbook.info/

[17] D. J. Bogucki, J. A. Domaradzki, R. E. Ecke, and C. R. Truman, "Light scattering on oceanic turbulence," *Applied optics*, vol. 43, no. 30, pp. 5662–5668, 2004.

[18] W. Liu, Z. Xu, and L. Yang, "SIMO detection schemes for underwater optical wireless communication under turbulence," *Photon. Res.*, vol. 3, no. 3, pp. 48–53, Jun 2015. [Online]. Available: http://www.osapublishing.org/prj/abstract.cfm?URI=prj-3-3-48

[19] Z. Ghassemlooy, W. Popoola, and S. Rajbhandari, *Optical Wireless Communications: System and Channel Modelling with MATLAB*, 1st ed. USA: CRC Press, Inc., 2012.

[20] X. Liu, S. Yi, X. Zhou, Z. Fang, Z.-J. Qiu, L. Hu, C. Cong, L. Zheng, R. Liu, and P. Tian, "34.5 m underwater optical wireless communication with 2.70 Gbps data rate based on a green laser diode with nrz-ook modulation," *Opt. Express*, vol. 25, no. 22, pp. 27 937–27 947, Oct 2017. [Online]. Available: http://www.opticsexpress.org/abstract.cfm?URI=oe-25-22-27937

[21] C. Shen, Y. Guo, H. M. Oubei, T. K. Ng, G. Liu, K.-H. Park, K.-T. Ho, M.-S. Alouini, and B. S. Ooi, "20-meter underwater wireless optical communication link with 1.5 Gbps data rate," *Opt. Express*, vol. 24, no. 22, pp. 25 502–25 509, Oct 2016. [Online]. Available: http://www.opticsexpress.org/abstract.cfm?URI=oe-24-22-25502

[22] J. Liu, B. Zheng, L. Zhao, and Z. Gong, "A design of underwater wireless laser communication system based on PPM modulating method," in *OCEANS 2015 - MTS/IEEE Washington*, 2015, pp. 1–6.

[23] W. O. Popoola and Z. Ghassemlooy, "BPSK subcarrier intensity modulated free-space optical communications in atmospheric turbulence," *J. Lightwave Technol.*, vol. 27, no. 8, pp. 967–973, Apr 2009. [Online]. Available: http://jlt.osa.org/abstract.cfm?URI=jlt-27-8-967

[24] W. Popoola, Z. Ghassemlooy, C. Lee, and A. Boucouvalas, "Scintillation effect on intensity modulated laser communication systems—a laboratory demonstration," *Optics & Laser Technology*, vol. 42, no. 4, pp. 682–692, 2010. [Online]. Available: https://www.sciencedirect.com/science/article/pii/S0030399209002461

[25] W. Cox, J. A. Simpson, and J. Muth, "Underwater optical communication using software defined radio over LED and laser based links," *2011 - MILCOM 2011 Military Communications Conference*, pp. 2057–2062, 2011.

[26] H. G. Olanrewaju, J. Thompson, and W. O. Popoola, "Pairwise coding for MIMO-OFDM visible light communication," *IEEE Transactions on Wireless Communications*, vol. 19, no. 2, pp. 1210–1220, 2020.

[27] B. Krongold, K. Ramchandran, and D. Jones, "Computationally efficient optimal power allocation algorithms for multicarrier communication systems," *IEEE Transactions on Communications*, vol. 48, no. 1, pp. 23–27, 2000.